



Communication

# Chelator PBT2 Forms a Ternary $\text{Cu}^{2+}$ Complex with $\beta$ -Amyloid That Has High Stability but Low Specificity

Simon C. Drew <sup>1,2</sup>

<sup>1</sup> Brain–Immune Communication Lab, Institut Pasteur, Université Paris Cité, F-75015 Paris, France; sdrew@pasteur.fr or sdrew@unimelb.edu.au

<sup>2</sup> Department of Medicine (Royal Melbourne Hospital), The University of Melbourne, Victoria 3010, Australia

**Abstract:** The metal chelator PBT2 (5,7-dichloro-2-[(dimethylamino)methyl]-8-hydroxyquinoline) acts as a terdentate ligand capable of forming binary and ternary  $\text{Cu}^{2+}$  complexes. It was clinically trialed as an Alzheimer’s disease (AD) therapy but failed to progress beyond phase II. The  $\beta$ -amyloid ( $\text{A}\beta$ ) peptide associated with AD was recently concluded to form a unique  $\text{Cu}(\text{A}\beta)$  complex that is inaccessible to PBT2. Herein, it is shown that the species ascribed to this binary  $\text{Cu}(\text{A}\beta)$  complex in fact corresponds to ternary  $\text{Cu}(\text{PBT2})\text{N}_{\text{Im}}^{\text{A}\beta}$  complexes formed by the anchoring of  $\text{Cu}(\text{PBT2})$  on imine nitrogen ( $\text{N}_{\text{Im}}$ ) donors of His side chains. The primary site of ternary complex formation is His6, with a conditional stepwise formation constant at pH 7.4 ( $^{\circ}\text{K} [\text{M}^{-1}]$ ) of  $\log^{\circ}K = 6.4 \pm 0.1$ , and a second site is supplied by His13 or His14 ( $\log^{\circ}K = 4.4 \pm 0.1$ ). The stability of  $\text{Cu}(\text{PBT2})\text{N}_{\text{Im}}^{\text{H13/14}}$  is comparable with that of the simplest  $\text{Cu}(\text{PBT2})\text{N}_{\text{Im}}$  complexes involving the  $\text{N}_{\text{Im}}$  coordination of free imidazole ( $\log^{\circ}K = 4.22 \pm 0.09$ ) and histamine ( $\log^{\circ}K = 4.00 \pm 0.05$ ). The 100-fold larger formation constant for  $\text{Cu}(\text{PBT2})\text{N}_{\text{Im}}^{\text{H6}}$  indicates that outer-sphere ligand–peptide interactions strongly stabilize its structure. Despite the relatively high stability of  $\text{Cu}(\text{PBT2})\text{N}_{\text{Im}}^{\text{H6}}$ , PBT2 is a promiscuous chelator capable of forming a ternary  $\text{Cu}(\text{PBT2})\text{N}_{\text{Im}}$  complex with any ligand containing an  $\text{N}_{\text{Im}}$  donor. These ligands include histamine, L-His, and ubiquitous His side chains of peptides and proteins in the extracellular milieu, whose combined effect should outweigh that of a single  $\text{Cu}(\text{PBT2})\text{N}_{\text{Im}}^{\text{H6}}$  complex regardless of its stability. We therefore conclude that PBT2 is capable of accessing  $\text{Cu}(\text{A}\beta)$  complexes with high stability but low specificity. The results have implications for future AD therapeutic strategies and understanding the role of PBT2 in the bulk transport of transition metal ions. Given the repurposing of PBT2 as a drug for breaking antibiotic resistance, ternary  $\text{Cu}(\text{PBT2})\text{N}_{\text{Im}}$  and analogous  $\text{Zn}(\text{PBT2})\text{N}_{\text{Im}}$  complexes may be relevant to its antimicrobial properties.

**Keywords:** 8-hydroxyquinoline; PBT2; amyloid; copper; ternary; terdentate; antimicrobial



**Citation:** Drew, S.C. Chelator PBT2 Forms a Ternary  $\text{Cu}^{2+}$  Complex with  $\beta$ -Amyloid That Has High Stability but Low Specificity. *Int. J. Mol. Sci.* **2023**, *24*, 9267. <https://doi.org/10.3390/ijms24119267>

Academic Editor: Giovanni Musci

Received: 1 May 2023

Revised: 18 May 2023

Accepted: 22 May 2023

Published: 25 May 2023



**Copyright:** © 2023 by the author. Licensee MDPI, Basel, Switzerland. This article is an open access article distributed under the terms and conditions of the Creative Commons Attribution (CC BY) license (<https://creativecommons.org/licenses/by/4.0/>).

## 1. Introduction

The compound 5,7-dichloro-2-[(dimethylamino)methyl]-8-hydroxyquinoline (PBT2) is a terdentate  $\text{Cu}^{2+}$  and  $\text{Zn}^{2+}$  chelator that was previously trialed as a therapeutic to treat Alzheimer’s disease (AD). Its anticipated mechanism of action was based on the controversial “metals hypothesis”, which proposed that AD results from aberrant interactions of the  $\beta$ -amyloid ( $\text{A}\beta$ ) peptide with endogenous transition metal ions, notably  $\text{Cu}^{2+}$ , causing  $\text{A}\beta$  to misfold and generate reactive oxygen species (ROS) [1,2]. PBT2 was proposed to prevent these interactions, sequester transition metal ions thought to be trapped within extracellular  $\beta$ -amyloid aggregates, and then enable cellular uptake of these ions by ionophore action [3]. However, repeated phase II clinical trials ultimately provided no evidence for cognitive efficacy of PBT2 in patients with prodromal or mild AD [4,5].

Using electron paramagnetic resonance (EPR) spectroscopy, the  $\text{Cu}^{2+}$  coordination of this class of ligand (L) was first characterized using the non-chlorinated homologue of PBT2 (Figure 1), which was shown to form a terdentate  $\text{CuL}$  complex and a five-coordinate

$\text{CuL}_2$  complex [6]. The proposed structure of  $\text{CuL}_2$  has been replicated in the crystal structure of PBT2 [7], and the UV–vis and EPR spectroscopic properties of  $\text{Cu}(\text{PBT2})$  and  $\text{Cu}(\text{PBT2})_2$  have been shown to mirror those of the non-chlorinated homologue [6–9] (Table S1). Early EPR studies also showed that both ligands form ternary  $\text{CuLN}_{\text{Im}}^{\text{X}}$  complexes (Figure 1) in which the labile  $\text{Cl}^-$  ligand of  $\text{CuL}$  is replaced with an imine ( $\text{N}_{\text{Im}}$ ) donor ligand provided by  $\text{X} =$  imidazole, histamine, L-His, or proteins such as  $\alpha$ -synuclein and  $\text{A}\beta$  (see, in particular, Figure S33 of ref. [6]). However, despite recently identifying a similar EPR spectroscopic signature using a  $\text{Cu}/\text{PBT2}/\text{A}\beta_{1-42}$  mixture, George and co-workers ascribed the signal to a unique PBT2-inaccessible  $\text{Cu}(\text{A}\beta)$  species and concluded that there was no evidence to support formation of a ternary  $\text{Cu}^{2+}$  complex [10]. Since this could be interpreted by some as a reason for the failure of PBT2 in AD clinical trials, it is important to resolve this contradiction.

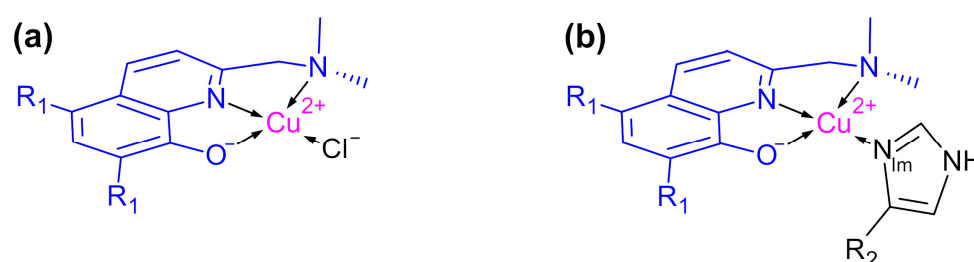


**Figure 1.** Structure of (a) binary and (b) ternary  $\text{Cu}^{2+}$  complexes of PBT2 ( $\text{R}_1 = \text{Cl}$ ) and its non-chlorinated homologue ( $\text{R}_1 = \text{H}$ ). The imine nitrogen ( $\text{N}_{\text{Im}}$ ) is supplied by ligands including imidazole ( $\text{R}_2 = \text{H}$ ), histamine ( $\text{R}_2 = \text{CH}_2\text{CH}_2\text{NH}_3^+$ ), L-His ( $\text{R}_2 = \text{CH}_2(\text{COO}^-)\text{CHNH}_3^+$ ), and His side chains ( $\text{R}_2 = \text{protein}$ ).

To address the above issue, we used EPR spectroscopy to analyze the species distributions in  $\text{Cu}/\text{PBT2}/\text{A}\beta$  mixtures in unprecedented detail and identify the number and stabilities of ternary  $\text{Cu}(\text{PBT2})\text{N}_{\text{Im}}^{\text{X}}$  complexes formed with  $\text{X} = \text{A}\beta_{1-40}$ .

## 2. Results

To characterize the  $\text{Cu}^{2+}$  complexes formed by PBT2 in the presence of  $\text{A}\beta$ , we titrated an equimolar mixture of PBT2 and  $\text{A}\beta_{1-40}$  in PBS pH 7.4 with  $\text{Cu}^{2+}$  and acquired the corresponding EPR spectra (Figure 2a). To determine the species distribution, each spectrum was decomposed into a linear superposition of basis spectra (Figure 2b) corresponding to  $\text{Cu}(\text{PBT2})$ ,  $\text{Cu}(\text{PBT2})_2$ ,  $\text{Cu}(\text{A}\beta_{1-40})$ ,  $\text{Cu}_2(\text{A}\beta_{1-40})$ , and the putative  $\text{Cu}(\text{PBT2})\text{N}_{\text{Im}}^{\text{A}\beta}$  complex. The spectrum of  $\text{Cu}(\text{PBT2})$  was obtained at equimolar  $\text{Cu}/\text{PBT2}$  stoichiometry and that of  $\text{Cu}(\text{PBT2})_2$  at sub-stoichiometric ratios (Figure S1). The spectra of  $\text{Cu}(\text{A}\beta)$  and  $\text{Cu}_2(\text{A}\beta)$  were acquired at  $\text{Cu}/\text{A}\beta$  ratios of 1:1 and 2.5:1 (Figure S2). Attempts to use linear combinations of normalized  $\text{Cu}(\text{PBT2})$ ,  $\text{Cu}(\text{PBT2})_2$ ,  $\text{Cu}(\text{A}\beta)$ , and  $\text{Cu}_2(\text{A}\beta)$  spectra failed to reproduce the EPR spectra of  $\text{Cu}/\text{PBT2}/\text{A}\beta_{1-40}$   $n$ :1:1 ( $n = 0$ –2.67), indicating that additional species must be formed. Indeed, the dominant spectral features did not resemble any of those of the above four species (Figure 2b and Figure S3). Rather, they corresponded closely to those of previously characterized  $\text{CuLN}_{\text{Im}}$  complexes (Table 1) [6,8,11], indicating that  $\text{Cu}(\text{PBT2})$  can anchor on the imine nitrogen ( $\text{N}_{\text{Im}}$ ) of the His side chains of  $\text{A}\beta_{1-40}$ .

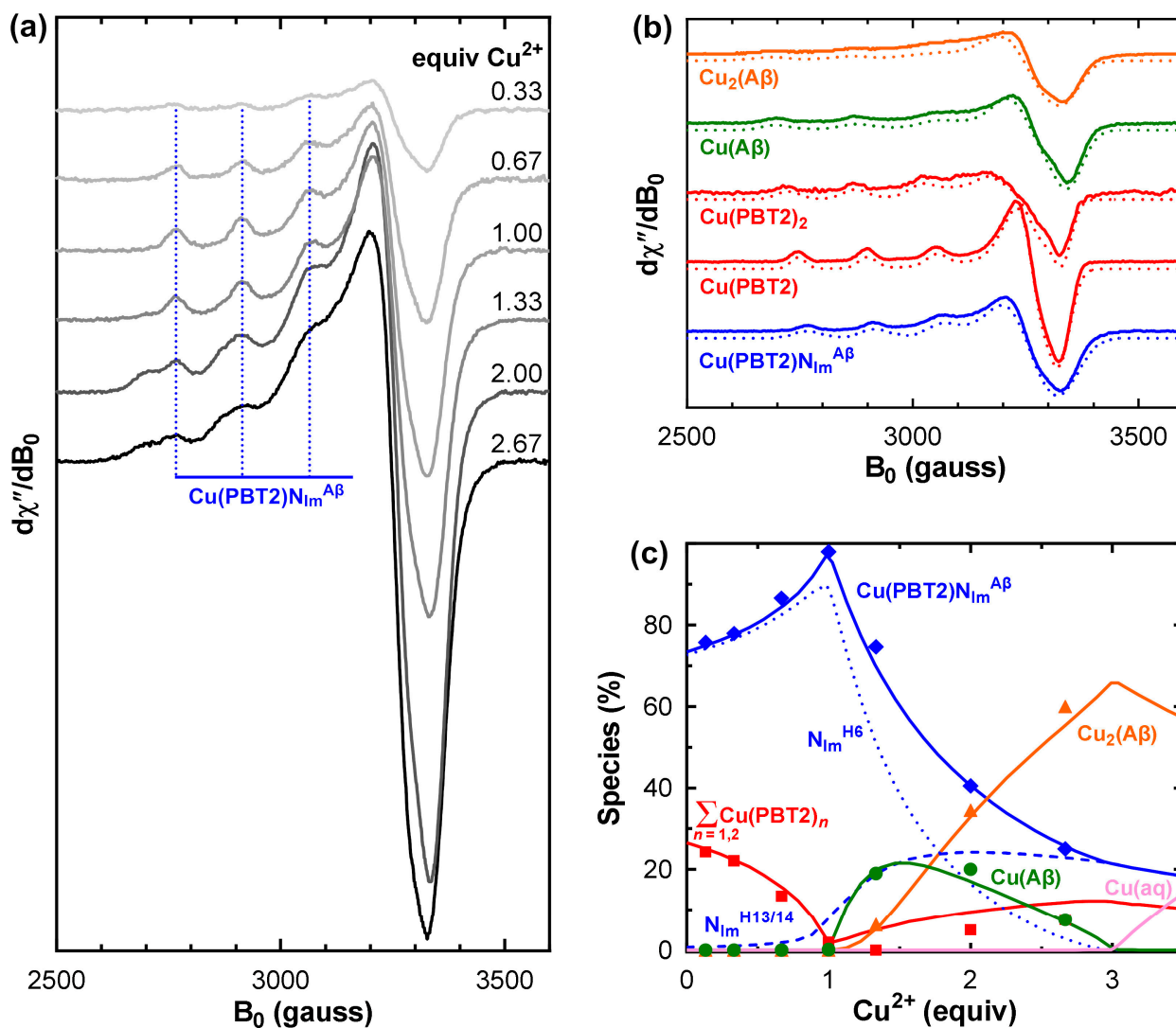


**Figure 2.** Determination of the number and stabilities of ternary  $\text{Cu(PBT2)(A}\beta_{1-40})$  interactions. (a) EPR spectra of  $^{65}\text{Cu/PBT2/A}\beta_{1-40}$   $n:1:1$  ( $n = 0.1\text{--}2.67$ ) in PBS pH 7.4 (0.2 mM PBT2/ $\text{A}\beta_{1-40}$ ). The group of vertical lines indicates the  $^{65}\text{Cu}$  hyperfine splitting ( $A_z$ ) associated with  $\text{Cu(PBT2)N}_{\text{Im}}^{\text{A}\beta}$ . (b) Normalized basis set (solid lines) used for the decomposition of the spectra in panel a (see Figures S1–S3 for details). Dotted lines show spectra simulated using the parameters in Table 1. The  $\text{Cu}_2(\text{A}\beta_{1-40})$  simulation is a weighted summation of spectra obtained using “first site” parameters (50%) and “second site” parameters (50%). Vertical scales in panels a and b are different. (c) Experimental species distributions (points) resulting from normalization and decomposition of the spectra in panel a (Figure S4), and theoretical distributions (solid lines) calculated using the relevant formation constants in Table 2 (see also Figure S5 for a comparison of relative and absolute  $\text{Cu}^{2+}$  speciation). The solid blue line in panel c shows the sum of  $\text{Cu(PBT2)N}_{\text{Im}}^{\text{H6}}$  (dotted line) and  $\text{Cu(PBT2)N}_{\text{Im}}^{\text{H13/14}}$  (dashed line).  $\text{Cu(aq)}$  denotes aqueous  $\text{Cu}^{2+}$  (pink). Experimental conditions: temperature, 77 K; microwave power, 10 mW; microwave frequency, 9.425 GHz; modulation amplitude, 8 G; sweep time, 84 s; time constant, 82 ms; averages, 4.

**Table 1.** Principal electron Zeeman ( $g_z$ ) and nuclear hyperfine ( $A_z$ ) parameters of binary and ternary  $\text{Cu}^{2+}$  complexes of PBT2 and its non-chlorinated homologue with  $\text{A}\beta_{1-40}$  and other imidazole-bearing ( $\text{N}_{\text{Im}}$ ) co-ligands. A detailed comparison with previously obtained parameters is shown in Table S1.

Complex	$g_z$	$A_z$ ( $^{63}\text{Cu}$ ) <sup>a</sup>	Reference
L = PBT2			
CuL	$2.259 \pm 0.002$	$151 \pm 1$	This work <sup>b</sup>
CuL <sub>2</sub>	$2.283 \pm 0.002$	$148 \pm 3$	This work <sup>b</sup>
CuLN <sub>Im</sub> <sup>X</sup>			
X = $\text{A}\beta_{1-40}$	$2.249 \pm 0.002$	$147 \pm 2$	This work <sup>b</sup>
X = imidazole	$2.248 \pm 0.001$	$143 \pm 1$	This work <sup>b</sup>
X = histamine	$2.248 \pm 0.001$	$143 \pm 1$	This work <sup>b</sup>
X = $\text{A}\beta_{1-42}$	$2.242 \pm 0.002$	$142 \pm 3$	10 <sup>c</sup>
L = non-chlorinated PBT2 homologue			
CuL	$2.255 \pm 0.001$	$153 \pm 1$	6
CuL <sub>2</sub>	$2.267 \pm 0.001$	$149 \pm 1$	6
CuLN <sub>Im</sub> <sup>X</sup>			
X = imidazole	$2.245 \pm 0.001$	$144 \pm 1$	This work <sup>b</sup> , 6, 11
X = histamine	$2.245 \pm 0.001$	$145 \pm 1$	This work <sup>b</sup> , 6, 11
$\text{A}\beta$			
Cu( $\text{A}\beta_{1-40}$ )	$2.268 \pm 0.002$	$174 \pm 2$	This work <sup>d</sup>
Cu <sub>2</sub> ( $\text{A}\beta_{1-40}$ )			
first site	$2.268 \pm 0.002$	$174 \pm 2$	This work <sup>e</sup>
second site	$2.309 \pm 0.005$	$168 \pm 5$	This work <sup>e</sup>

<sup>a</sup> Hyperfine parameters are expressed in units of  $10^{-4} \text{ cm}^{-1}$  ( $1 \times 10^{-4} \text{ cm}^{-1} = 2.9979 \text{ MHz}$ ). <sup>b</sup> To aid comparison with other studies, hyperfine couplings have been converted from those obtained using  $^{65}\text{Cu}$  to those expected for  $^{63}\text{Cu}$  using the scaling factor  $|g_n(^{63}\text{Cu})/g_n(^{65}\text{Cu})| = 1.07$ . <sup>c</sup> Species was not assigned to a ternary complex and spectral isolation was approximate. <sup>d</sup> Parameters are those for the dominant species at pH 7.4. <sup>e</sup> Coordination of the first-bound ion at the “first site” is assumed to be unperturbed by binding of a second ion at the “second site”.

**Table 2.** Stepwise conditional formation constants (pH 7.4) used to simulate the species distributions of  $\text{Cu}/\text{L}/\text{N}_{\text{Im}}^{\text{X}}$  mixtures for L = PBT2 and X =  $\text{A}\beta_{1-40}$  (Figure 2c), imidazole (Figure S6c), and histamine (Figure S9c). A detailed comparison of  $\text{Cu}^{2+}$  formation constants, including those for the non-chlorinated homologue of PBT2 and various  $\text{N}_{\text{Im}}$  donors, is provided in Table S2.

Complex	Formation Constant <sup>a</sup>	$\log[^c K/(1 \text{ M}^{-1})]$ at pH 7.4	Reference
CuL	$^c K_{\text{CuL}}^{\text{Cu}}$	$13.61 \pm 0.05$	8
CuL <sub>2</sub>	$^c K_{\text{CuL}_2}^{\text{CuL}}$	$5.95 \pm 0.07$	8
CuLN <sub>Im</sub> <sup><math>\text{A}\beta</math></sup> (His6)	$^c K_{\text{CuLN}_{\text{Im}}^{\text{H6}}}^{\text{CuL}}$	$6.4 \pm 0.1$	This work
CuLN <sub>Im</sub> <sup><math>\text{A}\beta</math></sup> (His13/14)	$^c K_{\text{CuLN}_{\text{Im}}^{\text{H13/14}}}^{\text{CuL}}$	$4.4 \pm 0.1$	This work
CuLN <sub>Im</sub> <sup>imidazole</sup>	$^c K_{\text{CuLN}_{\text{Im}}^{\text{imidazole}}}^{\text{CuL}}$	$4.22 \pm 0.09$	This work
CuLN <sub>Im</sub> <sup>histamine</sup>	$^c K_{\text{CuLN}_{\text{Im}}^{\text{histamine}}}^{\text{CuL}}$	$4.00 \pm 0.05$	This work
Cu( $\text{A}\beta_{1-40}$ )	$^c K_{\text{Cu}(\text{A}\beta)}^{\text{Cu}}$	$10.0 \pm 0.1$	This work
Cu <sub>2</sub> ( $\text{A}\beta_{1-40}$ )	$^c K_{\text{Cu}_2(\text{A}\beta)}^{\text{Cu}(\text{A}\beta)}$	$8.0 \pm 0.1$	This work

<sup>a</sup> Formation constants are defined in Equations (2)–(4) (Section 4.3).

To quantify the number and stabilities of ternary  $\text{Cu}(\text{PBT2})\text{N}_{\text{Im}}^{\text{A}\beta}$  interactions, it is important to consider how the His residues participate in binary  $\text{Cu}(\text{A}\beta)$  complexes. At pH 7.4,  $\text{Cu}(\text{A}\beta)$  is dominated by  $\{\text{NH}_2^{\text{D1}}, \text{C}=\text{O}^{\text{D1}}, \text{N}_{\text{Im}}^{\text{H6}}, \text{N}_{\text{Im}}^{\text{H13}}\}$  and  $\{\text{NH}_2^{\text{D1}}, \text{C}=\text{O}^{\text{D1}}, \text{N}_{\text{Im}}^{\text{H6}}, \text{N}_{\text{Im}}^{\text{H14}}\}$  coordination spheres with indistinguishable EPR spectra [12–14]. Thus, His6 is absolutely required to form  $\text{Cu}(\text{A}\beta)$ , whereas only one of His13 or His14 is needed. Thus, anchoring of  $\text{Cu}(\text{PBT2})$  on His6 to form  $\text{Cu}(\text{PBT2})\text{N}_{\text{Im}}^{\text{H6}}$  will occur at the expense of

Cu(A $\beta$ ), whereas anchoring on one of His13 or His14 to form Cu(PBT2)N<sub>Im</sub><sup>H13/14</sup> will not. Sequential binding of a second Cu<sup>2+</sup> ion by Cu(A $\beta$ ) generates Cu<sub>2</sub>(A $\beta$ ). The coordination in Cu<sub>2</sub>(A $\beta$ ) remains poorly defined, with one suggestion that binding of the second Cu<sup>2+</sup> ion changes the coordination of the first [15]. However, it will be shown below that a satisfactory explanation of the species distributions requires that His6 remains Cu<sup>2+</sup>-bound and His13 or His14 non-coordinated in Cu<sub>2</sub>(A $\beta$ ).

The conditional constants (<sup>c</sup>K) for formation of Cu(PBT2), Cu(PBT2)<sub>2</sub>, Cu(A $\beta$ ), and Cu<sub>2</sub>(A $\beta$ ) at pH 7.4 have all been previously determined (Table S2), which greatly simplified the task of determining the species distribution of the Cu/PBT2/A $\beta$ <sub>1–40</sub> *n*:1:1 system. Using these values and the EPR basis spectra (Figure 2b), we fitted the series of EPR spectra in Figure 2a as a function of the unknown constants <sup>c</sup>K<sub>CuLN<sup>H6</sup></sub><sup>CuL</sup> and <sup>c</sup>K<sub>CuLN<sup>H13/14</sup></sub><sup>CuL</sup> (see Section 4.3 for detail). The best agreement between the experimental and theoretical species distributions (Figure 2c) was obtained for log<sup>c</sup>K<sub>CuLN<sup>H6</sup></sub><sup>CuL</sup> = 6.4 ± 0.1 and log<sup>c</sup>K<sub>CuLN<sup>H13/14</sup></sub><sup>CuL</sup> = 4.4 ± 0.1 (Table 2). Allowing the conditional formation constants <sup>c</sup>K<sub>Cu(A $\beta$ )</sub><sup>Cu</sup> and <sup>c</sup>K<sub>Cu<sub>2</sub>(A $\beta$ )</sub><sup>Cu(A $\beta$ )</sup> to vary beyond their generally accepted ranges (Table S2) worsened the fit. Although we did not refine the value of <sup>c</sup>K<sub>CuL<sub>2</sub></sub><sup>CuL</sup>, we found that large changes from its published value (Table 2) also worsened the fit unless <sup>c</sup>K<sub>Cu(A $\beta$ )</sub><sup>Cu</sup> was set to a value beyond its accepted range.

The general appearance of the species distributions for Cu/PBT2/A $\beta$ <sub>1–40</sub> *n*:1:1 (Figure 2c and Figure S5) can be understood as follows: For small *n*, the 1000-fold greater stability of Cu(PBT2) compared with Cu(A $\beta$ ) (Table 2) ensures that Cu<sup>2+</sup> will first bind to PBT2, with the identity of the fourth in-plane ligand then being determined by the relative magnitudes of the stepwise constants <sup>c</sup>K<sub>CuLN<sup>H6</sup></sub><sup>CuL</sup> > <sup>c</sup>K<sub>CuL<sub>2</sub></sub><sup>CuL</sup> ≫ <sup>c</sup>K<sub>CuLN<sup>H13/14</sup></sub><sup>CuL</sup>. Thus, for *n* < 1, Cu<sup>2+</sup> is predominantly bound in a Cu(PBT2)N<sub>Im</sub><sup>H6</sup> complex with a minor quantity of Cu(PBT2)<sub>2</sub>. For *n* = 1, Cu(PBT2)<sub>2</sub> is almost entirely replaced by Cu(PBT2)N<sub>Im</sub><sup>H6</sup> and Cu(PBT2)N<sub>Im</sub><sup>H13/14</sup>, which only require one PBT2 molecule per Cu<sup>2+</sup> ion. For *n* > 1, with no free PBT2 molecules available, the additional Cu<sup>2+</sup> is coordinated in the next most stable binary complex, which is Cu(A $\beta$ ) (log<sup>c</sup>K<sub>Cu(A $\beta$ )</sub><sup>Cu</sup> = 10.0 ± 0.1). However, because Cu(A $\beta$ ) coordination requires His6, some Cu(PBT2) detaches from His6 and anchors instead on a His13 or His14 side chain, albeit with lower stability, to form Cu(PBT2)N<sub>Im</sub><sup>H13/14</sup>. As the available sites at His6 are gradually filled by Cu(A $\beta$ ), stepwise addition of a second Cu<sup>2+</sup> ion to the peptide occurs (log<sup>c</sup>K<sub>Cu<sub>2</sub>(A $\beta$ )</sub><sup>Cu(A $\beta$ )</sup> = 8.0 ± 0.1) to form Cu<sub>2</sub>(A $\beta$ ). Maximum occupancy of the Cu/PBT2/A $\beta$ <sub>1–40</sub> *n*:1:1 system is reached at *n* = 3, with two Cu<sup>2+</sup> ions bound to the “first” and “second” sites of A $\beta$ , and a third Cu<sup>2+</sup> ion bound either to Cu(PBT2) that is free (minor) or anchored to His13/14 of Cu<sub>2</sub>(A $\beta$ ) in a Cu(PBT2)N<sub>Im</sub><sup>H13/14</sup> complex (major).

More than three Cu<sup>2+</sup> ions cannot be accommodated by an equimolar PBT2/A $\beta$  mixture, with the excess Cu<sup>2+</sup> ions existing as aqueous copper that will precipitate as [Cu(OH)<sub>2</sub>]<sub>*n*</sub> at pH 7.4. Inclusion of Cu(PBT2)N<sub>Im</sub><sup>H13/14</sup>, whose formation does not depend on the Cu<sup>2+</sup> loading state of A $\beta$ , was essential to fit the experimental data. Alternative explanations of the physical origin of the lower-affinity ternary complex, such as a change in coordination of the first-bound Cu<sup>2+</sup> ion in Cu<sub>2</sub>(A $\beta$ ), can be ruled out because the concentration of Cu<sub>2</sub>(A $\beta$ ) relative to that of the ternary complex is too low at *n* < 2 (Figure S5).

The fact that <sup>c</sup>K<sub>CuLN<sup>H6</sup></sub><sup>CuL</sup> is 100-fold larger than <sup>c</sup>K<sub>CuLN<sup>H13/14</sup></sub><sup>CuL</sup> indicates that either Cu(PBT2)N<sub>Im</sub><sup>H6</sup> is stabilized by favorable outer-sphere ligand–peptide interactions and/or that Cu(PBT2)N<sub>Im</sub><sup>H13/14</sup> is destabilized by such interactions. To distinguish between these possibilities, we repeated the EPR analyses using Cu/PBT2/X 1:1:*n* systems with relatively unstructured N<sub>Im</sub> donor ligands from X = imidazole (Figures S6–S8) and histamine (Figures S9–S11). The EPR spectra of the isolated ternary Cu(PBT2)N<sub>Im</sub><sup>X</sup> complexes were characterized by the same parameters as Cu(PBT2)N<sub>Im</sub><sup>A $\beta$</sup>  spectra (Table 1), confirming

that each of these ternary  $\text{Cu}^{2+}$  complexes involves monodentate  $\text{N}_{\text{Im}}$  coordination of the co-ligand (Figure 1). The difference between  ${}^cK_{\text{CuLN}_{\text{Im}}^{\text{imidazole}}}^{\text{CuL}}$  and  ${}^cK_{\text{CuLN}_{\text{Im}}^{\text{H13/14}}}^{\text{CuL}}$  was within experimental error, whereas  ${}^cK_{\text{CuLN}_{\text{Im}}^{\text{histamine}}}^{\text{CuL}}$  was slightly lower than these constants (Table 2). Thus, we may conclude that the stability of  $\text{Cu}(\text{PBT2})\text{N}_{\text{Im}}^{\text{H13/14}}$  is not strongly influenced by outer-sphere ligand–peptide interactions, whereas such interactions greatly enhance the stability of  $\text{Cu}(\text{PBT2})\text{N}_{\text{Im}}^{\text{H6}}$ .

To independently verify the EPR method for deriving the conditional formation constants, we also determined the stability of the ternary  $\text{Cu}^{2+}$  complex of the non-chlorinated homologue of PBT2 ( $\text{L}'$ ) with imidazole (Figures S12–S14) and compared the value with that previously determined using potentiometric titrations [11]. After pH correction of the absolute stability constants (Table S3),  ${}^cK_{\text{CuL}'\text{N}_{\text{Im}}^{\text{imidazole}}}^{\text{CuL}'}$  was not significantly different from that determined here using EPR (Table S2) and, similar to PBT2, slightly higher than  ${}^cK_{\text{CuL}'\text{N}_{\text{Im}}^{\text{histamine}}}^{\text{CuL}'}$  (Figures S15–S17).

### 3. Discussion

EPR spectroscopy isolated a common  $\text{Cu}(\text{PBT2})\text{N}_{\text{Im}}^{\text{A}\beta}$  spectrum (Figure S3) for both  $\text{Cu}(\text{PBT2})\text{N}_{\text{Im}}^{\text{H6}}$  and  $\text{Cu}(\text{PBT2})\text{N}_{\text{Im}}^{\text{H13/14}}$  because they have very similar first coordination spheres. Nevertheless, as has been shown for other terdentate  $\text{Cu}^{2+}$  chelators [16,17], ternary complexes with different  $\text{N}_{\text{Im}}$  donor ligands can be distinguished based on their distinct formation constants, which are determined by outer-sphere interactions to which continuous-wave EPR is typically insensitive. Importantly, the spectroscopic signature of  $\text{Cu}(\text{PBT2})\text{N}_{\text{Im}}^{\text{A}\beta}$  isolated here for  $\text{Cu}/\text{PBT2}/\text{A}\beta_{1-40}$   $n$ :1:1 closely matches that reported for the species isolated in  $\text{Cu}/\text{PBT2}/\text{A}\beta_{1-42}$  1:2:1 [10] (Table 1). In the latter study, the authors ascribed this to a unique PBT2-inaccessible  $\text{Cu}(\text{A}\beta)$  complex and concluded that there was no evidence for ternary complex formation. However, it is clear that  $\text{CuLN}_{\text{Im}}^{\text{X}}$  complexes with this spectroscopic signature are formed by PBT2 with a number of  $\text{N}_{\text{Im}}$  donor ligands X (Table 1 and Table S1). Moreover, we demonstrated the requirement for two such complexes— $\text{Cu}(\text{PBT2})\text{N}_{\text{Im}}^{\text{H6}}$  and  $\text{Cu}(\text{PBT2})\text{N}_{\text{Im}}^{\text{H13/14}}$ —with distinct stabilities (Table 2) to explain the species distributions of  $\text{Cu}/\text{PBT2}/\text{A}\beta_{1-40}$  mixtures. The relatively high stability of  $\text{Cu}(\text{PBT2})\text{N}_{\text{Im}}^{\text{H6}}$  compared with complexes formed with other  $\text{N}_{\text{Im}}$  donors might result from stabilizing pi–pi stacking of the aromatic rings of PBT2 and Phe4 or Tyr10, although a combination of electrostatic, steric, and hydrogen-bonding effects may contribute.

Despite the large ternary formation constant for  $\text{Cu}(\text{PBT2})\text{N}_{\text{Im}}^{\text{H6}}$ , PBT2 remains a promiscuous  $\text{Cu}^{2+}$  chelator because it is capable of forming a ternary  $\text{Cu}(\text{PBT2})\text{N}_{\text{Im}}$  complex with all  $\text{N}_{\text{Im}}$  donor ligands, including ubiquitous His side chains of peptides and proteins in the biological milieu, whose combined effect should outweigh that of a single  $\text{Cu}(\text{PBT2})\text{N}_{\text{Im}}^{\text{A}\beta}$  complex regardless of its stability. We therefore conclude that PBT2 is capable of accessing  $\text{Cu}(\text{A}\beta)$  complexes with high stability but low specificity. Potential functional implications of  $\text{Cu}(\text{PBT2})\text{N}_{\text{Im}}$  complexes have been discussed in our previous studies of the non-chlorinated PBT2 homologue. First, as an alternative to acting as a mobile ion carrier (ionophore) in a lipid membrane, endocytosis of extracellular proteins on which  $\text{Cu}(\text{PBT2})$  is anchored, followed by release of  $\text{Cu}^{2+}$  in low-pH and/or reducing intracellular compartments, may contribute to the bulk transport of these ions [6]. Second, their production of ROS in the presence of ascorbate [11], in addition to the modulation of cellular ROS signaling following exposure to this class of ligand [17], contrasts with the originally intended ROS-silencing function of PBT2 [18].

Recently, PBT2 has found renewed interest as an antimicrobial compound. Notably, a number of gram-positive bacteria become re-sensitized to previously resistant classes of antibiotics when these antibiotics are supplemented with PBT2 and  $\text{Zn}^{2+}$  in mouse models of wound healing [19] and pneumonia [20]. These results have been attributed to multiple bactericidal mechanisms associated with intracellular  $\text{Zn}^{2+}$  accumulation, including im-

pairment of Mn-dependent superoxide dismutase and production of ROS [21]. Although ligands generally have a greater affinity for  $\text{Cu}^{2+}$  compared with  $\text{Zn}^{2+}$  [22], the above effects were observed in response to co-administration of PBT2 (~1  $\mu\text{M}$ ) with an excess of  $\text{Zn}^{2+}$  (~100  $\mu\text{M}$ ). Therefore, it remains unclear whether ternary  $\text{Cu}(\text{PBT2})\text{N}_{\text{Im}}$  complexes may be formed under these conditions. However, given the ability of PBT2 to also form terdentate  $\text{Zn}^{2+}$  chelates [7], a contribution from analogous  $\text{Zn}(\text{PBT2})\text{N}_{\text{Im}}$  complexes to the antimicrobial activity of Zn/PBT2 may be speculated.

## 4. Materials and Methods

### 4.1. Sample Preparation

$\text{A}\beta_{1-40}$  (purity > 95%) was synthesized in the Peptide Technology Facility of the Bio21 Molecular Science and Biotechnology Institute, The University of Melbourne. The lyophilized peptide was dissolved at a nominal concentration of 1 mg/mL in 1,1,1,3,3,3-hexafluoroisopropanol and portioned, then the solvent was allowed to evaporate. The resulting peptide film was resuspended at 4 °C in 20% *v/v* 20 mM NaOH, 70% *v/v* ultrapure water (MilliQ; MERCK KGAA, Darmstadt, Germany), and 10% *v/v* 10 × phosphate-buffered saline (PBS; 10 mM phosphate buffer, 2.7 mM KCl, 137 mM NaCl; Sigma). After centrifugation at  $14,000 \times g$  for 15 min at 4 °C, the supernatant was retained and the peptide concentration was immediately determined using  $\epsilon_{214} = 74,925 \text{ M}^{-1}\text{cm}^{-1}$  [23]. A concentrated stock of  $^{65}\text{CuCl}_2$  was prepared by stirring  $^{65}\text{CuO}$  ( $^{65}\text{Cu}$ , >99%; Cambridge Isotope Laboratories, Tewksbury, MA, USA) in concentrated HCl, evaporating excess HCl under heat, then adding ultrapure water. PBT2 was synthesized as previously described [24], and a 1 mM stock solution was prepared by solubilizing the hydrochloride salt directly in PBS.

From the above stock solutions, PBT2 and then  $^{65}\text{CuCl}_2$  were added to portions of  $\text{A}\beta_{1-40}$  to achieve final molar Cu/PBT2/ratios of  $n:1$  ( $n = 0.33\text{--}2.67$ ) with  $[\text{A}\beta_{1-40}] = 200 \mu\text{M}$ . Control samples containing Cu/PBT2 0.5:1, Cu/PBT2 1:1, Cu/ $\text{A}\beta_{1-40}$  1:1, and Cu/ $\text{A}\beta_{1-40}$  2.5:1 were also prepared. Glycerol (10% *v/v*) was added to the Cu/PBT2 control samples to prevent formation of a concentrated solute phase upon freezing. Immediately after Cu addition, the final solution pH was measured using a micro-probe (Hanna Instruments, Villafranca Padovana, Italy) and adjusted using concentrated NaOH or HCl as required. Samples were transferred to quartz EPR tubes (SQ-707; ATS Life Sciences Wilmad, Vineland, NJ, USA) and snap-frozen in liquid nitrogen within two minutes of the Cu addition.

### 4.2. EPR Spectroscopy

X-band continuous-wave EPR spectra were acquired using a Bruker ESP380E spectrometer fitted with a rectangular  $\text{TE}_{102}$  microwave cavity and a quartz cold finger insert. Microwave frequencies were measured using an EIP Microwave 548A frequency counter and  $g$  factors calibrated against the  $\text{F}^+$  line in CaO ( $g = 2.0001 \pm 0.0002$ ) [25]. Experimental conditions are indicated in the figure captions. Background correction was performed by subtraction of the buffer-only spectrum.

The “pepper” function in EasySpin v.5.2.33 [26,27] was used to simulate basis spectra using the static Hamiltonian

$$H = \beta_e \mathbf{B}^T \cdot \mathbf{g} \cdot \mathbf{S} + \mathbf{S}^T \cdot \mathbf{A} \cdot \mathbf{I} - g_n \beta_n \mathbf{B}^T \cdot \mathbf{I} \quad (1)$$

where  $\mathbf{S}$  and  $\mathbf{I}$  are the electron and  $^{65}\text{Cu}$  nuclear vector spin operators,  $\mathbf{g}$  and  $\mathbf{A}$  are the  $3 \times 3$  electron Zeeman and  $^{65}\text{Cu}$  electron–nuclear hyperfine coupling matrices,  $\beta_e$  is the Bohr magneton,  $\beta_n$  is the nuclear magneton, and  $\mathbf{B}$  is the applied magnetic field vector. Rhombic symmetry or higher was assumed for  $\mathbf{g}$  and  $\mathbf{A}$ , with principal values of  $g_x$ ,  $g_y$ , and  $g_z$  and  $A_x$ ,  $A_y$ , and  $A_z$ , respectively. The principal values of  $\mathbf{g}$  and  $\mathbf{A}$  and the lineshape parameters ( $g$ – $A$  strain model) were varied iteratively using the “esfit” module in EasySpin to minimize the difference between the experimental and simulated spectra.

#### 4.3. Determination of the Ternary Formation Constants for Cu/PBT2/Aβ<sub>1-40</sub> Mixtures

We followed an approach similar to that recently used to determine the number and stabilities of ternary Cu(GHK)N<sub>Im</sub><sup>HSA</sup> complexes formed between human serum albumin (HSA) and glycy-L-histidyl-L-lysine (GHK) [26]. The Cu(PBT2)N<sub>Im</sub><sup>Aβ</sup> spectrum was assumed to be a superposition of the spectra of two ternary complexes. The first complex involved anchoring of Cu(PBT2) on the His6 side chain (N<sub>Im</sub><sup>H6</sup>), which is also required for Cu(Aβ) formation; the second involved anchoring on a side chain of either His13 or His14 (N<sub>Im</sub><sup>H13/14</sup>), which is not required for Cu(Aβ) or Cu<sub>2</sub>(Aβ) formation. Thus, Cu(Aβ) and Cu<sub>2</sub>(Aβ) can simultaneously accommodate an Cu(PBT2)N<sub>Im</sub><sup>H13/14</sup> complex but not a Cu(PBT2)N<sub>Im</sub><sup>H6</sup> complex. Under these assumptions, Cu/PBT2/Aβ<sub>1-40</sub> *n*:1:1 can be modeled as Cu/L/A/B *n*:1:1:1, where ligand L is PBT2, ligand A acts like Aβ, and ligand B is treated as an isolated N<sub>Im</sub><sup>H13/14</sup> donor. The relevant formation constants are:

$$\begin{aligned}\beta'_{1100} &= {}^cK_{CuL}^{Cu} \quad \text{for Cu(PBT2)} \\ \beta'_{1200} &= {}^cK_{CuL}^{Cu} \times {}^cK_{CuL_2}^{Cu} \quad \text{for Cu(PBT2)}_2 \\ \beta'_{1010} &= {}^cK_{CuA}^{Cu} \quad \text{for Cu(A}\beta\text{)} \\ \beta'_{1020} &= {}^cK_{CuA}^{Cu} \times {}^cK_{Cu_2A}^{Cu} \quad \text{for Cu}_2\text{(A}\beta\text{)} \\ \beta'_{1110} &= {}^cK_{CuL}^{Cu} \times {}^cK_{CuLA}^{Cu} \quad \text{for Cu(PBT2)N}_{Im}^{H6} \\ \beta'_{1101} &= {}^cK_{CuL}^{Cu} \times {}^cK_{CuLB}^{Cu} \quad \text{for Cu(PBT2)N}_{Im}^{H13/14}\end{aligned}\quad (2)$$

where the cumulative conditional (pH-dependent) constants ( $\beta'$ ) are defined by

$$\beta'_{pqrs} = \frac{[Cu_p L_q A_r B_s]}{[Cu]^p [L]^q [A]^r [B]^s} \quad \text{for } pCu + qL + rA + sB \rightleftharpoons Cu_p L_q A_r B_s \quad (3)$$

and the stepwise conditional formation constants ( ${}^cK$ ) are defined by

$$\begin{aligned}{}^cK_{CuX}^{Cu} &= \frac{[CuX]}{[Cu][X]} \quad \text{for } Cu + X \rightleftharpoons CuX \quad (X = L, A) \\ {}^cK_{CuLX}^{CuL} &= \frac{[CuLX]}{[CuL][X]} \quad \text{for } CuL + X \rightleftharpoons CuLX \quad (X = A, B) \\ {}^cK_{Cu_2A}^{CuA} &= \frac{[Cu_2A]}{[CuA][Cu]} \quad \text{for } CuA + Cu \rightleftharpoons Cu_2A.\end{aligned}\quad (4)$$

To determine the ternary formation constants  ${}^cK_{CuLA}^{CuL}$  and  ${}^cK_{CuLB}^{CuL}$ , we made use of the previously published values for  ${}^cK_{CuL}^{Cu}$ ,  ${}^cK_{CuL_2}^{Cu}$ ,  ${}^cK_{CuA}^{Cu}$ , and  ${}^cK_{Cu_2A}^{CuA}$  at pH 7.4 (Tables 2 and S2). Initial guesses for  ${}^cK_{CuLA}^{CuL}$  and  ${}^cK_{CuLB}^{CuL}$  were then made, and their values were systematically varied as follows:

- (1) For each value of  ${}^cK_{CuLA}^{CuL}$  and  ${}^cK_{CuLB}^{CuL}$ , the theoretical distributions of CuL, CuL<sub>2</sub>, CuA, Cu<sub>2</sub>A, CuLA, and CuLB were calculated for the condition Cu/PBT2/Aβ<sub>1-40</sub> 1:1:1  $\equiv$  Cu/L/A/B 1:1:1:1 under which spectral features attributable to the ternary species were maximal (Figure 2c).
- (2) The theoretical speciation in step 1 provided weighting factors that were used to algebraically subtract the normalized spectra of CuL, CuL<sub>2</sub>, and CuA (Figure 2b) from the experimental spectrum of Cu/PBT2/Aβ<sub>1-40</sub> 1:1:1  $\equiv$  Cu/L/A/B 1:1:1:1, thus yielding a weighted summation of indistinguishable CuLA and CuLB spectra.
- (3) Linear combinations of the normalized CuL, CuL<sub>2</sub>, CuA, Cu<sub>2</sub>A, CuLA, CuLB basis spectra were used to reconstruct the experimental EPR spectra at all intermediate stoichiometries Cu/PBT2/Aβ<sub>1-40</sub> *n*:1:1  $\equiv$  Cu/L/A/B *n*:1:1:1 (0.33  $\leq n \leq$  2.67), and the weightings were iteratively varied using a generalized reduced gradient nonlinear solver (Frontline Systems Inc., Incline Village, NV, USA) to minimize the root-mean-squared deviation between the reconstructions and the experimental spectra.
- (4) The deviation between the fitted and experimental values of [CuL], [CuL<sub>2</sub>], [CuA], [Cu<sub>2</sub>A], and [CuLN<sub>Im</sub><sup>Aβ</sup>] = [CuLA] + [CuLB] for all values of *n* was calculated.

- (5) New values of  ${}^cK_{\text{CuLA}}^{\text{CuL}}$  and  ${}^cK_{\text{CuLB}}^{\text{CuL}}$  were chosen and steps 1–4 were repeated until the root-mean-squared deviation was minimized.

The above method assumed that the frozen-solution EPR spectra of  $\text{Cu}(\text{PBT2})\text{N}_{\text{Im}}^{\text{H6}}$  and  $\text{Cu}(\text{PBT2})\text{N}_{\text{Im}}^{\text{H13/14}}$  are indistinguishable, which is justified by the identification of a common set of spin Hamiltonian parameters for numerous  $\text{Cu}(\text{PBT2})\text{N}_{\text{Im}}$  complexes with different  $\text{N}_{\text{Im}}$  donor ligands (Table 1 and Table S1). This assumption was also shown to be true for ternary  $\text{Cu}^{2+}$  complexes of different  $\text{N}_{\text{Im}}$  donors with other terdentate ligands such as the non-chlorinated homologue of PBT2 (Table S1), the GHK tripeptide [16,28], and  $\alpha$ -synuclein [29].

**Supplementary Materials:** The following supporting information can be downloaded at: <https://www.mdpi.com/article/10.3390/ijms24119267/s1>. References [30–33] are cited in the supplementary materials.

**Funding:** This research received no external funding.

**Data Availability Statement:** The data presented in this study are available on request from the corresponding author.

**Acknowledgments:** PBT2 was kindly supplied by Vijaya Kenche, Florey Institute of Neuroscience and Mental Health, Australia.

**Conflicts of Interest:** The author declares no conflict of interest.

## References

- Bush, A.I. Metals and neuroscience. *Curr. Opin. Chem. Biol.* **2000**, *4*, 184–191. [CrossRef] [PubMed]
- Bush, A.I. Drug development based on the metals hypothesis of Alzheimer's disease. *J. Alzheimers Dis.* **2008**, *15*, 223–240. [CrossRef] [PubMed]
- Adlard, P.A.; Bica, L.; White, A.R.; Nurjono, M.; Filiz, G.; Crouch, P.J.; Donnelly, P.S.; Cappai, R.; Finkelstein, D.I.; Bush, A.I. Metal ionophore treatment restores dendritic spine density and synaptic protein levels in a mouse model of Alzheimer's disease. *PLoS ONE* **2011**, *6*, e17669. [CrossRef] [PubMed]
- Sampson, E.L.; Jenagaratnam, L.; McShane, R. Metal protein attenuating compounds for the treatment of Alzheimer's dementia. *Cochrane Database Syst. Rev.* **2014**, *2*, CD005380. [CrossRef]
- Available online: [www.alzforum.org/news/research-news/pbt2-takes-dive-phase-2-alzheimers-trial](http://www.alzforum.org/news/research-news/pbt2-takes-dive-phase-2-alzheimers-trial) (accessed on 1 April 2014).
- Kenche, V.B.; Zawisza, I.; Masters, C.L.; Bal, W.; Barnham, K.J.; Drew, S.C. Mixed ligand  $\text{Cu}^{2+}$  complexes of a model therapeutic with Alzheimer's amyloid- $\beta$  peptide and monoamine neurotransmitters. *Inorg. Chem.* **2013**, *52*, 4303–4318. [CrossRef]
- Nguyen, M.; Vendier, L.; Stigliani, J.-L.; Meunier, B.; Robert, A. Structures of the Copper and Zinc Complexes of PBT2, a Chelating Agent Evaluated as Potential Drug for Neurodegenerative Diseases. *Eur. J. Inorg. Chem.* **2017**, *2017*, 600–608. [CrossRef]
- Sgarlata, C.; Arena, G.; Bonomo, R.P.; Giuffrida, A.; Tabbi, G. Simple and mixed complexes of copper(II) with 8-hydroxyquinoline derivatives and amino acids: Characterization in solution and potential biological implications. *J. Inorg. Biochem.* **2018**, *180*, 89–100. [CrossRef]
- Summers, K.L.; Roseman, G.P.; Sopsis, G.J.; Millhauser, G.L.; Harris, H.H.; Pickering, I.J.; George, G.N. Copper(II) Binding to PBT2 Differs from That of Other 8-Hydroxyquinoline Chelators: Implications for the Treatment of Neurodegenerative Protein Misfolding Diseases. *Inorg. Chem.* **2020**, *59*, 17519–17534. [CrossRef]
- Summers, K.L.; Roseman, G.; Schilling, K.M.; Dolgova, N.V.; Pushie, M.J.; Sokaras, D.; Kroll, T.; Harris, H.H.; Millhauser, G.L.; Pickering, I.J.; et al. Alzheimer's Drug PBT2 Interacts with the Amyloid  $\beta$  1–42 Peptide Differently than Other 8-Hydroxyquinoline Chelating Drugs. *Inorg. Chem.* **2022**, *61*, 14626–14640. [CrossRef]
- Mital, M.; Zawisza, I.A.; Wiloch, M.Z.; Wawrzyniak, U.E.; Kenche, V.; Wróblewski, W.; Bal, W.; Drew, S.C. Copper Exchange and Redox Activity of a Prototypical 8-Hydroxyquinoline: Implications for Therapeutic Chelation. *Inorg. Chem.* **2016**, *55*, 7317–7319. [CrossRef]
- Drew, S.C.; Barnham, K.J. The Heterogeneous Nature of  $\text{Cu}^{2+}$  Interactions with Alzheimer's Amyloid- $\beta$  Peptide. *Acc. Chem. Res.* **2011**, *44*, 1146–1155. [CrossRef] [PubMed]
- Faller, P.; Hureau, C.; La Penna, G. Metal ions and intrinsically disordered proteins and peptides: From Cu/Zn amyloid- $\beta$  to general principles. *Acc. Chem. Res.* **2014**, *47*, 2252–2259. [CrossRef] [PubMed]
- Drew, S.C.; Noble, C.J.; Masters, C.L.; Hanson, G.R.; Barnham, K.J. Pleomorphic copper coordination by Alzheimer's amyloid- $\beta$  peptide. *J. Am. Chem. Soc.* **2009**, *131*, 1195–1207. [CrossRef] [PubMed]
- Alies, B.; Renaglia, E.; Rózga, M.; Bal, W.; Faller, P.; Hureau, C. Cu(II) affinity for the Alzheimer's peptide: Tyrosine fluorescence studies revisited. *Anal. Chem.* **2013**, *85*, 1501–1508. [CrossRef]
- Bossak-Ahmad, K.; Bal, W.; Fraczyk, T.; Drew, S.C. Ternary  $\text{Cu}^{2+}$  Complexes of Human Serum Albumin and Glycyl-L-histidyl-L-lysine. *Inorg. Chem.* **2021**, *60*, 16927–16931. [CrossRef]

17. Bossak-Ahmad, K.; Wiśniewska, M.; Bal, W.; Drew, S.C.; Fraczyk, T. Ternary Cu(II) complex with GHK peptide and cis-urocanic acid as a potential physiologically functional copper chelate. *Int. J. Mol. Sci.* **2020**, *21*, 6190. [[CrossRef](#)]
18. Drew, S.C. The case for abandoning therapeutic chelation of copper ions in Alzheimer's disease. *Front. Neurosci.* **2017**, *11*, 317. [[CrossRef](#)]
19. Bohlmann, L.; De Oliveira, D.M.P.; El-Deeb, I.M.; Brazel, E.B.; Harbison-Price, N.; Ong, C.Y.; Rivera-Hernandez, T.; Ferguson, S.A.; Cork, A.J.; Phan, M.D.; et al. Chemical Synergy between Ionophore PBT2 and Zinc Reverses Antibiotic Resistance. *mBio* **2018**, *9*, e02391-18. [[CrossRef](#)]
20. Brazel, E.B.; Tan, A.; Neville, S.L.; Iverson, A.R.; Udagedara, S.R.; Cunningham, B.A.; Sikanyika, M.; De Oliveira, D.M.P.; Keller, B.; Bohlmann, L.; et al. Dysregulation of *Streptococcus pneumoniae* zinc homeostasis breaks ampicillin resistance in a pneumonia infection model. *Cell Rep.* **2022**, *38*, 110202. [[CrossRef](#)]
21. Harbison-Price, N.; Ferguson, S.A.; Heikal, A.; Taiaroa, G.; Hards, K.; Nakatani, Y.; Rennison, D.; Brimble, M.A.; El-Deeb, I.M.; Bohlmann, L.; et al. Multiple Bactericidal Mechanisms of the Zinc Ionophore PBT2. *mSphere* **2020**, *5*, e00157-20. [[CrossRef](#)]
22. Irving, H.; Williams, R.J.P. The stability of transition-metal complexes. *J. Chem. Soc.* **1953**, 3192–3210. [[CrossRef](#)]
23. Kuipers, B.J.H.; Gruppen, H. Prediction of Molar Extinction Coefficients of Proteins and Peptides Using UV Absorption of the Constituent Amino Acids at 214 nm To Enable Quantitative Reverse Phase High-Performance Liquid Chromatography-Mass Spectrometry Analysis. *J. Agric. Food Chem.* **2007**, *55*, 5445–5451. [[CrossRef](#)] [[PubMed](#)]
24. Barnham, K.J.; Gautier, E.C.L.; Kok, G.B.; Krippner, G. 8-Hydroxy quinoline derivatives. U.S. Patent 20080161353A1, 3 July 2008.
25. Wertz, J.E.; Orton, J.W.; Auzins, P. Electron spin resonance studies of radiation effects in inorganic solids. *Discuss. Faraday Soc.* **1961**, *31*, 140–150. [[CrossRef](#)]
26. Stoll, S.; Britt, R.D. General and efficient simulation of pulse EPR spectra. *Phys. Chem. Chem. Phys.* **2009**, *11*, 6614–6625. [[CrossRef](#)]
27. Stoll, S.; Schweiger, A. EasySpin, a comprehensive software package for spectral simulation and analysis in EPR. *J. Magn. Reson.* **2006**, *178*, 42–55. [[CrossRef](#)]
28. Haigh, C.L.; Tumpach, C.; Collins, S.J.; Drew, S.C. A 2-substituted 8-hydroxyquinoline stimulates neural stem cell proliferation by modulating ROS signalling. *Cell Biochem. Biophys.* **2016**, *74*, 297–306. [[CrossRef](#)]
29. Drew, S.C.  $\alpha$ -synuclein and  $\beta$ -amyloid form a bridged copper complex. *Appl. Magn. Reson.* **2015**, *46*, 1041–1052. [[CrossRef](#)]
30. Sarell, C.J.; Syme, C.D.; Rigby, S.E.; Viles, J.H. Copper(II) binding to amyloid-beta fibrils of Alzheimer's disease reveals a picomolar affinity: Stoichiometry and coordination geometry are independent of A $\beta$  oligomeric form. *Biochemistry* **2009**, *48*, 4388–4402. [[CrossRef](#)]
31. Kowalik-Jankowska, T.; Ruta, M.; Wiśniewska, K.; Lankiewicz, L. Coordination abilities of the 1-16 and 1-28 fragments of beta-amyloid peptide towards copper(II) ions: A combined potentiometric and spectroscopic study. *J. Inorg. Biochem.* **2003**, *95*, 270–282. [[CrossRef](#)]
32. Sjöberg, S. Critical evaluation of stability constants of metal-imidazole and metal-histamine systems (Technical Report). *Pure Appl. Chem.* **1997**, *69*, 1549–1570. [[CrossRef](#)]
33. Ringbom, A. The analyst and the inconstant constants. *J. Chem. Educ.* **1958**, *35*, 282–288. [[CrossRef](#)]

**Disclaimer/Publisher's Note:** The statements, opinions and data contained in all publications are solely those of the individual author(s) and contributor(s) and not of MDPI and/or the editor(s). MDPI and/or the editor(s) disclaim responsibility for any injury to people or property resulting from any ideas, methods, instructions or products referred to in the content.